ACS OMEGA

Open Access

http://pubs.acs.org/journal/acsodf

Article

Fast In Vitro Synthesis and Direct Labeling of Nanobodies for Prototyping in Microscopy Applications

Lukas Behrens, Ruben Magnus Walter, Weining Cai, Helge Ewers, Bas van Bommel,* and Anne Zemella*

Cite This: *ACS Omega* 2024, 9, 35374−35383

Read Online

ACCESS | Metrics & More | Article Recommendations | Supporting Information

ABSTRACT: Small antigen binders, such as nanobodies, have become widely used in biomedical research and pharmaceutical development. However, the pipeline for the generation of functional conjugated probes and drugs from identified binders remains a major time-consuming bottleneck. Here, we developed a method for fast nanobody production and conjugation based on an in vitro synthesis platform. Our system allows for small batch synthesis of nanobodies with the inclusion of a noncanonical amino acid (NCAA). This NCAA can then be used for direct conjugation of molecules to the synthesized nanobody using click-chemistry, reducing the time from binder-encoding DNA to a conjugated probe tremendously. In this study, we conjugated a fluorescent dye to an anti-Green fluorescent protein (GFP) nanobody and attained a fully functional probe suitable for advanced super-resolution microscopy within a short time frame of 2 days. Our work illustrates that an in vitro synthesis platform in combination with click-chemistry can be successfully employed to produce conjugated small antigen binding probes. The fast production and conjugation, combined with the possibility for parallelization as well as precise analysis by microscopy, forms an excellent platform for nanobody prototyping. The here-illustrated method can be used for quick selection and benchmarking of obtained nanobody sequences/clones, e. g., from a phage-display, for use as conjugated small-molecule carriers. This procedure can accelerate the bioengineering of nanobodies for research and pharmaceutical applications.

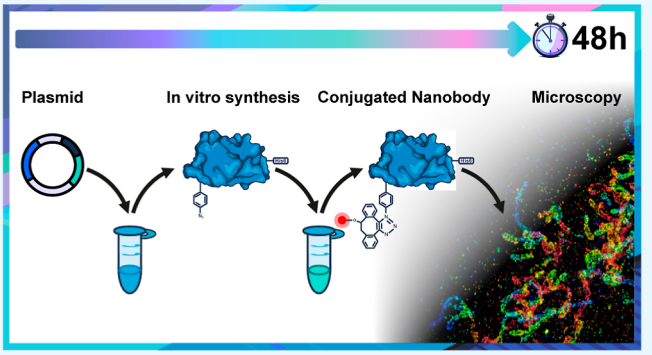

INTRODUCTION

Epitope-recognizing proteins such as antibodies have found a wide application in biotechnology. Especially nanobodies, small binders consisting of only the epitope-binding domains of heavy chain IgGs, as they are found in camelids, are sought after. Nanobodies are structured by a central disulfide bond and three variable antigen-binding loops that typically form the epitope-recognizing domain. They show strong potential for therapeutics as they can be easily produced; their small size leads to good tissue penetration and allows the recognition of more hidden epitopes. Moreover, their protein structure and the possibility to bioengineer their sequence can result in minimal activation of the immune system in vivo.[1] By conjugation, nanobodies form excellent small-molecule carriers that can provide advantages in a variety of applications.

Unique epitope-recognizing nanobody sequences are obtained from larger nanobody libraries by affinity-based selection. These libraries are constructed from nanobody sequences obtained from lymphocytes, after immunization of a host with a particular antigen.[2−4] At this time, fully synthetic or enhanced libraries are developed with the goal to enlarge or optimize the pool before selection.[5] The final epitope-recognizing nanobody sequences are obtained from the complex libraries by multiple rounds of selection/biopanning. These usually consist of multiple rounds of phage or ribosome display and further refinement by quantitative downstream assays. The resulting epitope-binding nanobodies can then be recombinantly expressed with high yields in bacteria and used as a small-molecule carrier. Stringent selection criteria during the search for binders often result in the identification of nanobodies with outstanding specifications. This includes higher solubility, pH stability, temperature stability, low immunogenicity, resistance against proteases, and high-association and low-dissociation constants.[1] These characteristics may be further improved by targeted mutagenesis.[2] At last, their small size inherently allows them to penetrate complex cellular structures and tissues readily through

Received: February 5, 2024
Revised: July 26, 2024
Accepted: July 26, 2024
Published: August 9, 2024

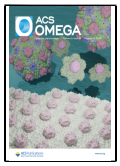

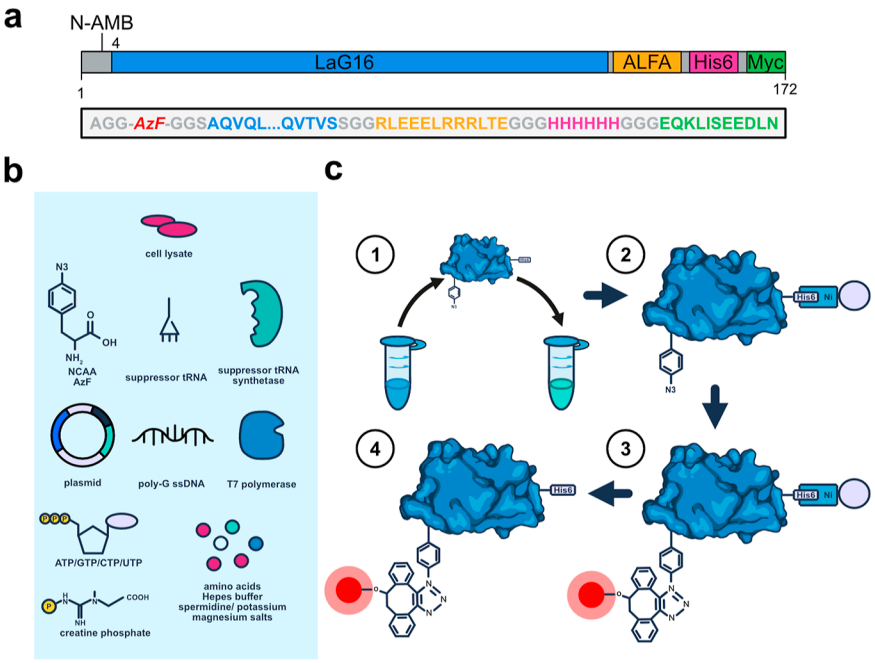

Figure 1. Schematic overview of the nanobody production, conjugation, and application workflow. (a) Graphical illustration of the synthesized nanobody sequence, indicating the position of the NCAA and additional tags. (b) Components of the in vitro transcription−translation reaction to produce the anti-GFP nanobody in a batch format within 3 h. (c) Illustrative depiction of the steps in nanobody purification and conjugation conducted directly after in vitro synthesis (1), its purification via magnetic Ni-NTA beads (2), the on-bead strain promoted alkyne−azide cycloaddition to site-specifically introduce an Alexa Fluor 647 fluorophore (3), and the elution of the conjugated nanobody as the final product (4).

diffusion. Their stringent selection, further protein engineering and inherent attributes make nanobodies outperform antibodies in certain applications. Well-performing nanobodies find a wide usage in pharmaceutical[6−9] and research[3,10−12] applications. Approved nanobody-based pharmaceutical treatments function by the inhibition of ligand−receptor binding (Envafolimab/Ozoralizumab),[6,8] the inhibition of protein binding and complex formation (Caplacizumab),[7] or the engineering of a functional high-affinity transmembrane receptor (Ciltacabtagene autoleucel).[9] New nanobody-based treatments may be approved for pharmaceutical use in the near future. In research applications, nanobodies have proven to be a valuable tool for biological discoveries through their benefits compared to antibodies.[13] Their small size, high target affinity, and short sequences offer benefits in expression and downstream microscopy applications, where it reduces unspecific labeling and labeling error (distance between the fluorophore and the actual protein target). This is of special importance in super-resolution microscopy where the localization accuracy is high.[3,10] Their short and often known sequence allows for bioengineering with the aim of improving their properties by targeted mutagenesis, humanization of the overall sequence, or incorporation of amino acids for later conjugation to other compounds. The latter characteristic entails an influence on the number of amino acids available for conjugation and their position as well as on the labeling ratio (conjugates/protein). Furthermore, a part of the identified nanobodies can also be expressed in eukaryotic cells as intrabodies, allowing for live cell studies.[11,13] The path of biopanning from library to identified epitope-binding nanobodies is a tedious effort; however, it enhances the selection of binders with outstanding performance. Hereby, nanobodies provide an excellent alternative or improvement in comparison to full-size antibodies.

When nanobodies are used as small-molecule carriers, in which, e. g., a fluorophore or pharmaceutical reagent is covalently attached, this conjugation poses additional challenges in terms of protein affinity, stability, and solubility. A panel of identified nanobody sequences from biopanning methods often requires additional experimentation to find suitable candidates that can carry the desired conjugates. The large size of conjugates relative to that of the nanobody might impede its functionality. Equally so, the position of the conjugate may also influence the abovementioned properties. Hence, site-directed labeling is of advantage as the interference with the epitope-binding of the very small (∼13 kDa) nanobody must be avoided, which is nearly impossible in semidirected labeling techniques based on, for example, succinimidyl esters or thioesters. However, site-directed labeling is difficult due to the limited options/positions in the short nanobody sequence, nonetheless possible by using targeted enzymatic methods or inclusion of noncanonical amino acids (NCAAs) combined with click-chemistry.[14,15] Suitable nanobody binders, as identified by biopanning methods, should ideally be tested in the conjugated state when this is required for their final application. The use of NCAAs in combination with click-chemistry is advantageous as they can be incorporated on different sites of the proteins, possibly replacing a naturally occurring amino acid. Hereby, the impact on the nanobody sequence can be minimized. Unfortunately, the use of NCAAs in large-scale bacterial expression is expensive, especially if a larger panel of binders requires testing. Here, we use a GFP-binding nanobody to develop a method for fast prototyping of nanobodies with site-directed conjugation.[2] To achieve this, we used in vitro synthesis for fast production and site-direct conjugation via click-chemistry on NCAAs.[16] In vitro synthesis, also called cell-free protein synthesis, is based on transcriptionally/transla-

https://doi.org/10.1021/acsomega.4c01164
ACS Omega 2024, 9, 35374−35383

tionally active lysates that were obtained from cultivated and homogenized cells. Lysates contain active transcription and translation machinery without the need of maintaining a living organism. We show the feasibility of our approach with proof-of-principle experiments using a well-characterized anti-GFP nanobody. We employed an optimized in vitro synthesis mix, based on a Chinese hamster ovary (CHO)-cell lysate, for the synthesis of clickable nanobodies in a fast and resource-efficient manner.[16] This approach led to a fully functional anti-GFP nanobody that showed great specificity in microscopy. This method could be used to characterize preliminary nanobody candidates for target specificity when carrying a small molecule payload. This in vitro approach allows for parallel expression of small batches of nanobodies in a short time frame while enabling easy extension of the canonical amino acid code with NCAAs. The sensitivity and high contrast of fluorescence microscopy together with rapid synthesis and click-chemistry based conjugation allows for fast and efficient prototyping of nanobody-conjugate candidates.

RESULTS

A key step in nanobody testing is validation against their target. Light microscopy, due to its precision and excellent contrast, is an extremely sensitive means for the validation of small-molecule binders such as nanobodies. However, nanobody production usually requires recombinant expression and purification before conjugation with compounds. This can take up to several days. We reasoned that the combination of in vitro synthesis and click-chemistry-based conjugation, via genetic code extension, could lead to fluorescently labeled nanobodies in a few hours, simplifying high-throughput testing. For validating this approach, we used the coding sequence for the LaG16 anti-GFP nanobody and inserted the UAG Amber stop codon into a short N-terminal linker sequence for later conjugation via a NCAA inserted here (referred to as N-AMB construct) (Figure 1a).[2] We also added a His6-tag to the C-terminus of the nanobody to ensure that only fully functional nanobodies containing the NCAA would be synthesized and purified via Ni-NTA beads. Besides the Amber stop codon and the His6-tag, our construct included both a Myc- and an ALFA-tag for possible downstream applications such as binding assays.[12] For incorporation of the NCAA, we added recombinantly purified *t*-RNA recognizing the Amber UAG stop codon that was specifically bound to the NCAA L-4-azidophenylalanine (AzF) in the transcription−translation mix.[16] This mix was based on a cell lysate from CHO cells genome-edited to express a *t*-RNA synthetase recognizing the Amber-specific *t*-RNA (Figure 1b). It was furthermore spiked with AzF, additional amino acids, T7 polymerase, energy sources, and poly-G ssDNA in a HEPES-based buffer. When we ran this reaction in a heat block at 30 °C, we could extract nanobodies using magnetic Ni-NTA beads after 3 h. Following extensive washing, the nanobodies could be conjugated directly on the beads to Alexa Fluor 647 (AF647) DIBO using copper-free click-chemistry,[14] removing unbound dye by washes on the beads (Figure 1c). This reaction is, of course, compatible with many other conjugation reagents or chemistries.

We next aimed to test the production and labeling efficiency of the nanobody including the N-AMB sequence in comparison to the native protein. We ran four reactions: one sample missing the template (no-template control), one sample containing the coding sequence for the native nanobody without an Amber stop codon, and two samples including the Amber stop codon in the coding sequence. In all reactions, we included ^{14}C-labeled leucine for qualitative and quantitative radioactive detection. We then immobilized the products on Ni-NTA beads, washed them and performed a click-reaction on the incorporated AzF, washed again and eluted them from the Ni-NTA beads. During the course of this, we added AF647-DIBO for reaction with AzF in only one of the samples expressing the Amber stop codon-containing nanobody. The other N-AMB-including sample served as an unconjugated control. When we ran all four products on a PAGE gel and examined them by autoradiography (Figure 2a).

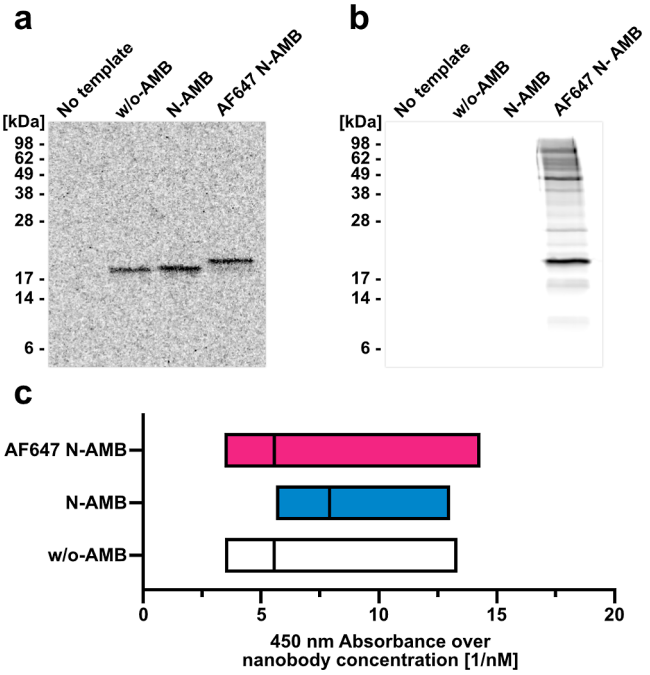

Figure 2. Autoradiography, in-gel fluorescence, and quantitative ELISA of the in vitro-synthesized and dye-conjugated nanobody. (a) Autoradiography of the elution fractions for all conditions. Size standards are indicated to the left. Estimating the apparent size shift between the Alexa Fluor 647-modified (20.25 ± 0.21 kDa, theoretically 20.55 kDa) and unmodified N-AMB (18.44 ± 0.20 kDa, theoretically 18.66 kDa) based on said size standards reveals a 1.81 ± 0.29 kDa gap (Alexa Fluor 647 DIOB weighing approximately 1.9 kDa). (b) In-gel fluorescence from the same gel region shown in (a) with a Cy5 filter set. Size standards are derived again from the SeeBlue Plus 2 protein ladder. (c) Nanobody-binding affinity quantified via an ELISA dilution series and depicted as concentration normalized absorbance. The bars cover 95% confidence intervals and medians calculated according to Fieller.[32]

We found that the reactions containing cDNA were similarly productive (Lanes 2 and 3) and that, as expected, additional AF647-coupling caused a slight shift in molecular mass (Lane 4). The quantitative shift of the AF647-coupled nanobody band demonstrates the high efficiency of the labeling reaction. As expected, we did not detect any products after the Ni-NTA pulldown from a reaction containing no template (Lane 1).

When we imaged the same gel for AF647 fluorescence, we found that besides the expected and dominant band at the known size for the AF647-conjugated nanobody, we also detected several bands of other proteins that exhibited AF647 fluorescence (Figure 2b). As these bands did not exhibit an ^{14}C

https://doi.org/10.1021/acsomega.4c01164
ACS Omega 2024, 9, 35374−35383

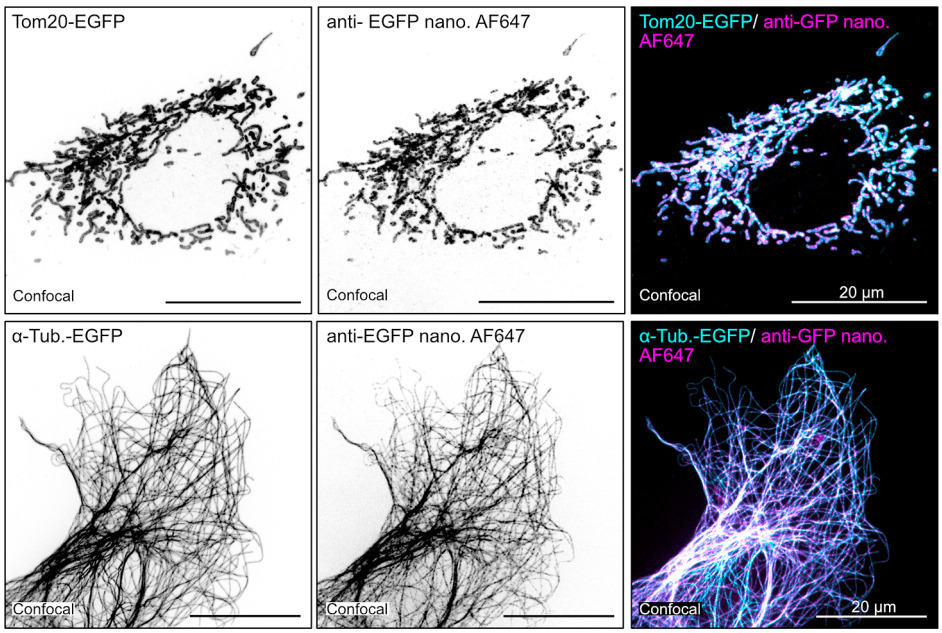

Figure 3. Immunocytochemistry staining with in vitro-synthesized and conjugated nanobodies in confocal microscopy. Anti-EGFP immunocytochemistry with in vitro-synthesized nanobodies against overexpressed TOM20-EGFP labeling mitochondria and α-tubulin outlining the microtubule cytoskeleton. Max intensity projections of confocal stacks.

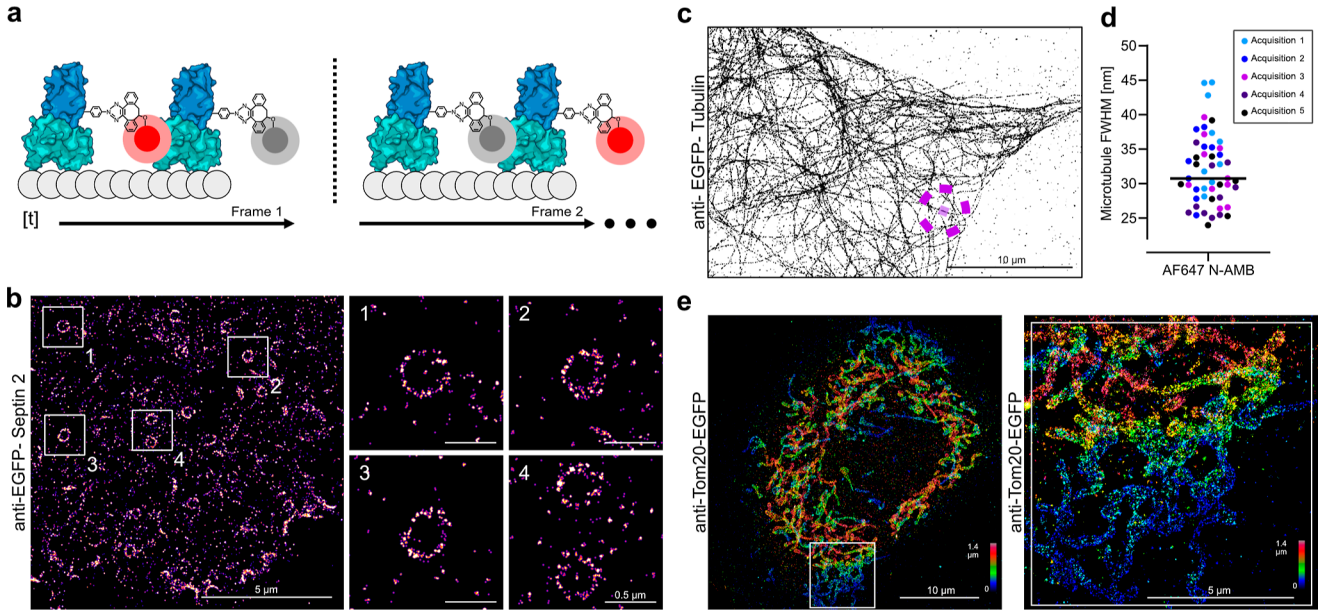

Figure 4. SMLM acquisitions and quantification with the in vitro-synthesized, dye-conjugated nanobody. (a) Application of the synthesized nanobody in SMLM via stochastic activation of the fluorophores and acquisition by multiple frames. (b) SMLM-acquired image of cytochalasin-D-treated EGFP-Septin 2 knock-in cell line labeled by the in vitro-synthesized nanobody. (c) SMLM-acquired image of overexpressed α-tubulin-EGFP labeled by the in vitro-synthesized nanobody. (d) Quantification of the microtubule diameter measured as indicated in purple in (c). (e) Left, 3D-SMLM acquisition of overexpressed TOM20-EGFP outlining the mitochondrial network. Right, zoom-in of the region indicated in the left image.

signal, we concluded that these bands might result from proteins present in the in vitro synthesis mix that bound unspecifically to the Ni-NTA beads and in some way reacted with AF647 DIBO.

We next aimed to test whether or not the site-directed conjugation of the AF647 dye to the nanobody or the incorporation of the NCAA would impede the nanobody-binding capability. Therefore, we performed an ELISA immunoassay targeting GFP. We found that the binding of all expressed and purified nanobody constructs was similar (Figure 2c). We concluded that in vitro synthesis in combination with NCAA incorporation can produce functional nanobodies that can bind to their target molecules.

The obtained results encouraged us to perform more sensitive testing to rule out nonspecific binding of involuntarily labeled byproducts from previous steps. To do so, we performed high-resolution microscopy experiments on specific targets in fixed cells. We overexpressed the EGFP-tagged

https://doi.org/10.1021/acsomega.4c01164
ACS Omega 2024, 9, 35374−35383

mitochondrial marker TOM20 and EGFP-tagged α-tubulin in NRK52E and COS-7 cells, respectively. After 24 h of expression, the cells were fixed with paraformaldehyde and processed for immunocytochemistry (see Materials and Methods). The cells were incubated overnight with the AF647-conjugated in vitro-synthesized nanobody. When we imaged the samples by volumetric spinning disk confocal microscopy in the channels of EGFP and AF647 fluorescence, we found that the transfected constructs lead to highly specific and high contrast labeling of mitochondria (TOM-20-EGFP) and microtubules (α-tubulin-EGFP) (Figure 3).

In the AF647 channel, we could observe highly specific staining of the very same structures in maximum z-projections, indicating that the in vitro-synthesized nanobody bound specifically to its GFP-target with minimal background. This precision was dependent on the nanobody's binding specificity as cells incubated with the unconjugated dye (Alexa Fluor 647 DIBO) displayed unspecific background staining, possibly caused by unspecific labeling of proteins or through hydrophobic membrane interactions (Supporting Information Figure S1). This unspecific staining was strongly reduced when the dye was clicked to a NCAA. In such experiments, unspecific staining by the unconjugated dye might be avoided by using other conjugates or alternative reactive click-chemistry groups.[17] When labeling cells with our dye-conjugated nanobody, we did not experience such off-target background, which indicates that any potentially troubling unbound dye was removed by washes during the purification of the conjugated nanobody from the Ni-NTA beads. From the accurate staining, we concluded that our AF647 site-specific-conjugated nanobody was an efficient probe and is a suitable carrier that can bring AF647 to its GFP target molecule.

In the next set of experiments, we further challenged the functionality of the in vitro-synthesized nanobody. Hence, additional samples were now processed for single-molecule localization microscopy (SMLM) (Figure 4a). We performed dSTORM, in which samples are incubated in a reducing/oxygen removing buffer for induction of stochastic activation and thereby on/off switching of AF647, a dye that excels in SMLM. The stochastic activation of the fluorophores allows for their sequential detection followed by computational fitting of their emission peaks, resulting in highly accurate localization in the sample. From the cumulative localizations over many imaging cycles, super-resolved images can be reconstructed. To generate our first target, we treated our NRK52E-EGFP-Septin 2 endogenous expressing knock-in cell line with cytochalasin D for the induction of Septin rings.[18,19] This NRK52E EGFP-Septin 2 cell line shows the expression of Septin 2 at endogenous levels with EGFP attached to its N-terminus. From experience, we know that cytochalasin D-induced actin destabilization prompts the formation of Septin rings, which can be resolved by SMLM microscopy. Similar to the other targets, these ring-structures built from Septins were well labeled and could be easily super-resolved with our in vitro-synthesized nanobody as performed before (Figure 4b).[19] We next prepared samples similar to the confocal experiments, where we expressed EGFP coupled to α-tubulin and TOM20 in COS-7 and NRK52E cells. These samples allowed us to quantify the labeling accuracy of the nanobody and offered larger structures for 3D-SMLM. The nanobody, with its small size, showed excellent labeling of the microtubule network (Figure 4c). Quantification of the microtubule diameter (FWHM) showed a small labeling error as expected, in line with other work (Figure 4d).[3,10] Since our nanobody displayed excellent molecular brightness, we additionally performed 3D-SMLM of mitochondria (Figure 4e). Our results show that an in vitro-synthesized and direct conjugated nanobody can be efficiently used for super-resolution microscopy applications in 2D and 3D.

DISCUSSION

Here, we demonstrate a fast, reproducible, and resource-efficient method for the production of nanobodies combined with site-directed conjugation. Our method has the potential to be efficiently parallelized for the screening of nanobody sequences and clones. The method thus offers the potential to speed up the final rounds of nanobody selection, where the focus lies on fast and efficient testing of a panel of identified binders for downstream assays.[2] In this way, it can make the screening of functional conjugated probes more time- and resource efficient. For the in vitro synthesis of the GFP nanobody in this work, we found typical yields of 100−150 ng/mL, which were sufficient for performing downstream microscopy assays. From experience, we know that protein yield can vary significantly between different polypeptide sequences and can also be higher for nanobodies.[20] For this work, we used a eukaryotic lysate, in which we established the expression of proteins with NCAAs. For the expression of nanobodies with NCAAs, prokaryotic lysates might be an alternative and could be tested to potentially increase the yields. However, it will be challenging to realize yields achieved by purification from larger-scale bacterial cultures. The method presented here is fast, precise, and resource friendly. This comes with lower yields as a trade-off. This method can find its use in prototyping/testing of nanobody-conjugate sequences, where one aims to find the best working sequence for microscopy or pharmaceutical applications. The best-performing nanobody could then be produced in higher quantity by other methods.[20]

We demonstrate the use of our in vitro-synthesized and conjugated nanobodies in a highly sensitive application, microscopy and especially super-resolution microscopy, where even minute amounts of unfunctional or badly conjugated binders generate significant background and error.[21,22] For this purpose, we conjugated the fluorescent dye AF647 via click-chemistry to an in vitro-expressed anti-GFP nanobody utilizing an incorporated NCAA. The conjugation site was designed near the N-terminus, distanced via a linker sequence from the epitope-binding site, to ensure efficient binding despite the conjugation of payloads. This position of the suppressed stop codon for NCAA incorporation also ensured that only nanobodies containing NCAA were purified via the C-terminal His6-tag. The final obtained conjugated nanobody performed excellently, as observed by confocal and localization-based super-resolution microscopy, showing the benefits of a highly specific small binder and a reduced labeling error in these applications.

Besides the approach we took in this proof-of-principle study, a similar protocol could be used with other sites for NCAA incorporation and click-chemistry reactive groups. In the past, we had excellent experience with enzyme-based C-terminal conjugation, which should also be possible using in vitro synthesis.[14] C-terminal conjugation via NCAAs may result in the synthesis of significantly more nonconjugatable nanobodies as byproduct, as termination at the Amber stop codon will generate nanobodies with only small differences in

https://doi.org/10.1021/acsomega.4c01164
ACS Omega 2024, 9, 35374−35383

molecular mass. While this would not deplete the in vitro synthesis mix from components for biosynthesis, it may make it harder to purify functional and conjugatable nanobodies. A premature stop in translation of the N-terminal tagged nanobody will result in an almost neglectable byproduct of 3 amino acids, while a C-terminal tagged synthetic construct may form functional binding nanobodies that lack NCAAs. In microscopy applications like here, N-terminal NCAA labeling may be preferred as it will reduce the risk of epitope occupation by nonconjugated nanobodies, carried over by a unintended incomplete purification. This would negatively impact the fluorescent labeling of the target. Given the right approach, we hypothesize that directed conjugation could be used for more microscopy applications, like quantitative 1-to-1 labeling for super-resolution microscopy or as a consistent maker for molecule orientation of solitary proteins or complexes.[23−26] This could be useful for electron microscopy, where ultrastructural information on proteins is obtained by the alignment of numerous molecules.[27] A conjugate at a selected position in the protein structure may function as an alignment landmark and equally so, in MINFLUX and high magnification expansion microscopy which have been shown to achieve single protein resolution.[17,23,24] Furthermore, we point out that the in vitro transcription−translation reaction in combination with the incorporation of NCAAs is not limited to small proteins such as nanobodies, as we demonstrated in this work. Other small epitope binders such as Affimers, DARPins, fibronectin-based binders, etc., may be candidates.[13,28−30] This also holds true for larger proteins, which can be equally produced via in vitro synthesis with the incorporation of NCAAs. The combination of site-directed conjugation with in vitro synthesis opens up a variety of opportunities in the biotechnological production, screening, and benchmarking of proteinaceous-conjugates.

Our method has its strengths in the final steps of protein engineering, where one seeks to test the functionality of a protein conjugate in its final application with high precision. In this study, we employed high-end microscopy techniques, although the applications may be easily expanded. There is a large repertoire of chemical reagents that can be clicked copper-free to NCAAs. This ranges from fluorescent molecules to pharmaceutical reagents, which could have properties that influence the hydrophobicity and epitope binding of the overall conjugate.[31] This may be of special importance for small binders since the conjugates are of relatively large size. The fast in vitro production and conjugation will help in the screening of epitope binders for their use in challenging applications. The relatively short time frame and low material costs allow for efficient experimentation and will accelerate technological biodevelopment and discovery.

MATERIALS AND METHODS

Nanobody Sequence. The in vitro-synthesized nanobody sequence based on Fridy et al. (Lag16 anti-GFP):[2]

w/o AMB. AGG____GGSAQVQLVESGGRLVQAGDSLRLSCAASGRTFSTSAMAWFRQAPGREREFVAAITWTVGNTILGDSVKGRFTISRDRAKNTVDLQMDNLEPEDTAVYYCSARSRGYVLSVLRSVDSYDYWGQGTQVTVSSGGSRLEEELRRRLTEGGGHHHHHHGGGEQKLISEEDLN.

With N-AMB. AGG-AzF-GGSAQVQLVESGGRLVQAGDSLRLSCAASGRTFSTSAMAWFRQAPGREREFVAAITWTVGNTILGDSVKGRFTISRDRAKNTVDLQMDNLEPEDTAVYYCSARSRGYVLSVLRSVDSYDYWGQGTQVTVSSGGSRLEEELRRRLTEGGGHHHHHHGGGEQKLISEEDLN.

The DNA sequences were codon optimized for mammalian expression and synthesized by Biocat.

In Vitro Synthesis and Click Reaction. The in vitro transcription−translation mix was composed as follows: 40% (v/v) orthogonal *p*-azido-L-phenylalanyl-*t*RNA synthetase expressing CHO lysate,[16] 30 *m*M HEPES-KOH (pH = 7.6) (BioMol GmbH, cat. no. 05288.1), 10 μM poly guanine (biomers.net GmbH), 100 μM canonical amino acids (Merck KGaA; see Table 1 below), 250 μM spermidine (Merck KGaA, cat. no. 85558-1G), 3.9 mM magnesium acetate (Merck KGaA, cat. no. 1.05819.1000), 135 mM potassium acetate (Merck KGaA, cat. no. 1.04820.1000), 30 μM ^{14}C-labeled L-leucine (200 dpm/pmol) (PerkinElmer Inc., cat. no. NEC279E001MC), 5 μM orthogonal suppressor tRNA, 2 mM *p*-azido-L-phenylalanine (AzF) (Iris Biotech GmbH, cat. no. HAA4090), 1 U/μL T7 RNA polymerase (Agilent Technologies, cat. no. 60012451), 20 μg/mL creatine phosphokinase (Roche Deutschland GmbH, cat. no. 247716221), 20 mM creatine phosphate (Roche Deutschland GmbH, cat. no. 10621714001), 1.75 mM ATP (Roche Deutschland GmbH, cat. no. 06529194), 0.3 mM GTP (Roche Deutschland GmbH, cat. no. 06529216), 0.3 mM CTP (Roche Deutschland GmbH, cat. no. 06529208), and 0.3 mM UTP (Roche Deutschland GmbH, cat. no. 06529224). The addition of ^{14}C-labeled L-leucine was omitted for the microscopy samples. Nevertheless, we ran a 50 μL reaction including ^{14}C-labeled L-leucine in parallel to verify the success of the transcription−translation reaction and to estimate the final nanobody yields. All steps after the addition of photosensitive AzF[33] were carried out avoiding light exposure.

The in vitro transcription−translation reaction was carried out in 50−60 μL batches at 30 °C with shaking at 500 rpm for 3 h. Afterward, these batches were pooled and subjected to

Table 1. Supplier Information for All Amino Acids Used for the In Vitro Synthesis Reaction

amino acid	supplier	cat. no.
Ala	Merck KGaA	1.01007.0100
Arg	Merck KGaA	1.01542.0100
Asn	Merck KGaA	1.01566.0100
Asp	Merck KGaA	1.00126.0100
Cys	Merck KGaA	1.02838.0100
Gln	Merck KGaA	1.00289.0100
Glu	Merck KGaA	1.00291.0100
Gly	Merck KGaA	1.04201.0100
His	Merck KGaA	1.04351.0005
Ile	Merck KGaA	1.05362.0100
Leu	Merck KGaA	1.05360.0100
Lys	Merck KGaA	1.12233.0100
Met	Merck KGaA	1.05757.0025
Phe	Merck KGaA	1.07256.0100
Pro	Merck KGaA	1.07434.0100
Ser	Merck KGaA	1.07769.0100
Thr	Merck KGaA	1.08411.0100
Trp	Merck KGaA	1.08374.0100
Tyr	Merck KGaA	1.08371.0100
Val	Merck KGaA	1.08495.0100

https://doi.org/10.1021/acsomega.4c01164
ACS Omega 2024, 9, 35374−35383

centrifugation at 4 °C and 16,000*g* for 15 min, removing the dispersed microsomes.

Pre-equilibrated Ni-NTA magnetic agarose beads [f.c. 0.125% (v/v), Qiagen, cat. no. 36113] were diluted in 4 volumes of binding buffer (300 mM NaCl, 50 mM NaH_2PO_4, 5 mM imidazole, and 0.05% Tween-20 in PBS), adding 1 volume of clear supernatant from the centrifugation. This suspension was then mixed thoroughly, and set for binding at 25 °C, with shaking at 900 rpm for 30 min.

Immediately afterward, one washing step with binding buffer and two additional steps in washing buffer (300 mM NaCl, 50 mM NaH_2PO_4, 20 mM imidazole, 0.05% Tween-20 in PBS) followed: 2 min each at 25 °C, with shaking at 900 rpm.

Click reactions were carried out on the beads overnight (18 h) at 25 °C, with shaking at 900 rpm in 50 μL of 50 μM Click-iT Alexa Fluor 647 DIBO alkyne (Thermo Fisher Scientific, cat. no. C10408) in PBS-T (0.05% Tween-20 in PBS). Negative controls were similarly treated in plain PBS-T.

Click reactions shown in Supporting Information Figure S1 were carried out overnight (18 h) at 25 °C, with shaking at 400 rpm in PBS. AzF/NCAA was added in a 1000-fold molar excess.

Washing was performed as described above, once with binding and then twice with washing buffer. Then, a two-step elution procedure in 50 μL of elution buffer (300 mM NaCl, 50 mM NaH_2PO_4, 250 mM imidazole, 0.05% Tween-20 in PBS) each at 25 °C, with shaking at 900 rpm for 10 min, was conducted.

The eluate was then transferred to a fresh 10 kDa MWCO Amicon Ultra-0.5 column (Merck, cat. no. UFC5010), and PBS was added at 300 μL followed by centrifugation at 4 °C and 15,000*g* for 30 min. More PBS was added ad 300 μL, the flow-through discarded, and a similar centrifugation step was conducted two additional times. The last centrifugation was continued until a volume of approximately 30 μL was retained.

This retained volume was then either filled up to 100 μL with PBS for immediate use (scintillation, autoradiography, and ELISA) or diluted in a storage buffer [2 mg/mL BSA (VWR, cat. no. 9048-46-8) and 50% (v/v) glycerol in PBS] for long-term storage and transport to the microscopy facility.

Liquid Scintillation Counting. To estimate the nanobody concentration attained by the respective in vitro transcription−translation reaction, a Hidex 600 SL liquid scintillation counter was employed. 25 μL of the ^{14}C-labeled final nanobody product was diluted with 3 mL of Quicksafe A scintillation cocktail (Zinsser Analytic, cat. no. 1008000) in a scintillation vial (Sarstedt, cat. no. 73.680) and mixed thoroughly in a shaker at 250 rpm for 30 min and then rested at least 15 min before scintillation counting. The applied volume was reduced to 15 μL per sample for the ELISA experiment.

All scintillation measurements were conducted as triplets using the average number of counts for the mathematical concentration determination.

In-Gel Fluorescence and Autoradiography. A 25 μL portion of the ^{14}C-labeled final nanobody product was mixed with NuPAGE 4x LDS loading buffer (f.c.: 1x, Thermo Fisher Scientific, cat. no. NP0008) supplemented with DTT (f.c.: 50 mM). The mixture was incubated at 70 °C for 10 min, with shaking at 1000 rpm, then cooled to room temperature (RT) and carefully spun down.

Polyacrylamide gels (4% w/v stacking, 14% w/v resolving gel) were prepared using the SureCast system kit (Thermo Fisher Scientific, cat. no. HC1000SR). The gels were used in combination with freshly prepared Novex 1x Tris-glycine running buffer (Thermo Fisher Scientific, cat. no. LC26755).

Each sample was loaded entirely onto the aforementioned polyacrylamide gel, and 10 μL of SeeBlue Plus2 Prestained Protein Standard (Thermo Fisher Scientific, cat. no. LC5925) was applied as a size reference. SDS-PAGE was then run in the prepared tris-glycine running buffer at 150 V for 70 min.

Afterward, the gel was rinsed twice with demineralized water and placed onto the fluorescence platform of an Amersham Typhoon 5 (GE Healthcare, cat. no. 29187191) biomolecular imager for in-gel fluorescence detection. For the Alexa Fluor 647 labeling experiments, the Cy5 fluorescence configuration of the biomolecular imager was used.

After washing another three times with demineralized water, the gel was subjected to 10 min of Coomassie staining in SimplyBlue SafeStain solution (Thermo Fisher Scientific, cat. no. LC6060) at RT after microwaving for 1 min with 600 W. Destaining was accomplished by washing three times with demineralized water, each time including another microwaving step for 1.5 min with 600 W, leaving the last batch of desalted water on the gel after the microwaving step to incubate for a further 30 min while shaking at 90 rpm.

In preparation for the autoradiography, the destained gel was placed onto wet filter paper and dried under vacuum at 70 °C for 55 min. The dried gel was placed on a phosphor screen (General Electric Healthcare, cat. no. 29175523) in an exposure cassette for 7 days. The sample was screen scanned using an Amersham Typhoon 5 (see above) in phosphor-imager mode to obtain the autoradiograph.

ELISA. One day before the nanobody samples were eluted, a fresh Costar Assay 96-well high bind plate (Corning, cat. no. CLS9018-100EA) was coated with 48 μL per well of 1.333 μg/mL EGFP-GST in coating buffer (100 mM Na_2CO_3, pH = 9.6) or plain coating buffer for no-antigen-control wells. Coating took place in the dark at 4 °C overnight.

The coating solution was removed from each well, followed by three washes with 200 μL of PBS-T [0.05 (v/v) % Tween-20 in PBS] per well. Blocking was conducted using 200 μL of freshly prepared 2% BSA (VWR, cat. no. 422381B) in PBS per well, incubated at RT for 2 h with shaking at 250 rpm in the dark. Afterward, the blocking solution was removed, and each well was washed three times with 200 μL of PBS-T.

Immediately after the blocking step was finished, a dilution series of each nanobody sample was prepared in binding buffer [1% (w/v) BSA in PBS]. Dilution steps included 1:20, 1:40, 1:80, 1:160, and 1:320 of the original nanobody concentration. Each dilution was then distributed in 50 μL triplicates to the corresponding wells on the ELISA plate. Nanobody binding occurred while protected from light at 4 °C overnight on a shaker at 250 rpm.

The radioactive binding fraction was carefully removed, and the samples were washed three times with 200 μL of PBS-T. For nanobody detection, a mouse anti-*c*-Myc primary antibody (Thermo Fisher Scientific, cat. no. 132500, Clone: 9E10) was used, diluted 1:1000 in binding buffer. 50 μL of diluted primary antibody was added to each well and then incubated at RT for 2 h with shaking at 250 rpm in the dark. Unbound primary antibody was removed by three washes with 200 μL of PBS-T each. Afterward, the samples were incubated with 50 μL of diluted goat anti-mouse HRP-conjugated secondary antibody (Azure Biosystems, cat. no. AC2115); diluted 1:2000 in binding buffer, binding at RT for 1 h while shaking at 250 rpm in the dark. Samples were finally washed three times with 200

https://doi.org/10.1021/acsomega.4c01164
ACS Omega 2024, 9, 35374−35383

μL of PBS-T and incubated with 50 μL of RT-acclimatized TMB single solution (Life Technologies, cat. no. 002023) at 250 rpm for 10 min. The reaction was stopped by adding 50 μL of 0.5 M sulfuric acid. Absorption at 450 nm was measured with an FLUOstar Omega SN 415 microplate reader (BMG Labtech).

Cloning Information. CMV-TOM20 (*Rattus norvegicus*)-EGFP-His10-tag was cloned by PCR amplification of TOM20-EGFP from a pAAV-Syn-TOM20 plasmid. The TOM20 sequence originated from a rat cDNA library.[11] His10-tag was included by PCR primer extension. The amplified fragment was cloned into a pEGFP-C1 vector by using restriction sites NheI (NEB, cat. no. R3131) and EcoRI (NEB, cat. no. R3101). The original EGFP in the pEGFP-C1 vector was thereby removed. The final sequence was verified by sanger sequencing.

CMV-EGFP-His10-tag-α-Tubulin (human TUBA1B) was cloned by PCR amplification of TUBA1B from a CMV-mCherry-TUBA1B plasmid. His10-tag was included by PCR primer extension. The amplified insert was placed into a pEGFP-C1 vector via restriction sites XhoI (NEB, cat. no. R0146) and KpnI (NEB, cat. no. R03142). The final sequence was verified by sanger sequencing.

Cell Culture. COS7 (DSMZ ACC60), NRK52E (ATCC, cat. no. CRL-1571), and NRK52E-EGFP-Septin $2^{EN/EN19}$ cell lines were cultured in DMEM (Thermo Fisher, cat. no. 31053-028) supplemented with 2 mM L-glutamine/GlutaMAX (Thermo Fisher, cat. no. 25030081/35050-061), 10% heat-inactivated fetal bovine serum (NeuFroxx, cat. no. 2095ML500), and Pen/Strep (Thermo Fisher, cat. no. 15140122). Cells were passaged twice per week with 0.25% trypsin/EDTA (Thermo Fisher, cat. no. 25200-072) and cultured to a maximum of 25 passages at 37 °C and 5% CO_2. Transfections were performed with Lipofectamine 3000 (Thermo Fisher, cat. no. L3000008). Cultures were frequently tested for mycoplasma by DAPI staining and PCR.

Immunocytochemistry. For microscopy, cells were grown on glass coverslips with a thickness of 1.5 (Marienfeld, cat. no. 0117550). Prior to use, the coverslips were cleaned for 10 min with a plasma cleaner. Cells were seeded directly onto glass coverslips; no additional coating was applied.

For fixed cell microscopy, cells were fixed with 4% PFA (Electron Microscopy Sciences., cat. no. 15710) and 0.25% glutaraldehyde (Electron Microscopy Sciences, cat. no. 16316) in PBS at 37 °C. For microtubule stainings, the cells were pre-extracted with 0.1% triton-X-100 (VWR, cat. no. 0694-1L) in PHEM buffer at 37 °C. For imaging of Septin 2 rings, the NRK52E-EGFP-Septin 2 cells were treated for 30 min with 5 μM cytochalasin D (Cayman Chemical, cat. no. 11330) in cell culture medium. The NRK52E-EGFP-Septin 2 cells were fixed with 4% PFA in PBS at 37 °C. Fixation buffers were removed with three washes with PBS, and then the cells were permeabilized with 0.2% triton-X-100 in PBS for 10 min. Next, the cells were blocked with blocking buffer (BB, 10% horse serum; Thermo Fisher Scientific, cat. no. 16050-130, 0.1% triton-X-100 in PBS) for 1 h at RT. Cells were incubated with the Alexa Fluor 647-conjugated nanobody in BB at 4 °C overnight. Next day, coverslips were washed three times with PBS. Samples were postfixed for 2−10 min with 4% PFA in PBS at RT. Finally, they were washed three times with PBS and then imaged in blinking buffer or mounted with Fluoromount-G including DAPI (Invitrogen, cat. no. 00-4959-52) for confocal microscopy.

For dye labeling experiments presented in Supporting Information Figure S1, NKR52E EGFP-Septin2 cells were treated for 30 min with 5 μM cytochalasin D prior to fixation. Cells were fixed with 4% PFA in PBS at 37 °C. The fixation buffer was removed with three washes with PBS. The cells were permeabilized with 0.2% triton-X-100 in PBS for 10 min. Next, the cells were blocked with BB for 1 h at RT. After blocking, the cells were incubated with no dye or 0.5 μM dye/conjugate in BB overnight at 4 °C. Unbound dye was removed by three washes with PBS. The samples were postfixed for 5 min with 4% PFA in PBS. Finally, the samples were washed three times with PBS and then imaged in PBS (confocal) or blinking buffer (dSTORM).

Microscopy. Confocal microscopy images were acquired using a Yokogawa CSU-X1-spinning-disk confocal microscope (Yokogawa). The confocal unit was attached to a Nikon Eclipse TI microscope body equipped with a 1.49 NA TIRF objective (Nikon, CFI APO TIRF 100XC Oil). The microscope was controlled by using VisiView software (Visitron Systems). EGFP was excited with a 488 nm laser and Alexa Fluor 647 with a 647 nm laser. Emission light was collected through a quad-band dichroic mirror, followed by corresponding emission filters with a water-cooled back-illuminated CMOS camera (PCO, PCO.edge 4.2 bi). The final pixel size on the camera was 65 nm. Acquisitions were obtained as a z-stack with a 0.2 μm step size. Images are presented as maximum z-projection.

Confocal microscopy images shown in Supporting Information Figure S1 were acquired by using a Yokogawa CSU-X1-spinning-disk confocal microscope (Yokogawa). The confocal unit was attached to an Olympus microscope body equipped with a 1.42 NA objective (Olympus, PlanApo N 60x Oil). The microscope was controlled by MetaMorph software. EGFP was excited with a 488 nm laser and Alexa Fluor 647 with a 635 nm laser. Emission light was collected through a quad-band dichroic mirror, followed by corresponding emission filters with a CMOS camera (Hamamatsu, ORCA-Flash 4.0). The final pixel size on the camera was 90 nm. Acquisitions were obtained as a z-stack with 0.5 μm step size. Images are presented as a maximum-intensity z-projection.

Super-resolution acquisitions were obtained using a Vutara 352 (Bruker) microscope system configured in biplane mode. The system was equipped with a 60× objective (Olympus, APON60XOTIRF—1.49 NA—Oil) resulting in a pixel size of 96.63 nm. All acquisitions were performed in β-mercaptoethanol (Merck, cat. no. M6250) blinking buffer including catalase (Merck, cat. no. C3155) and glucose oxidase (Merck, cat. no. G0543). Fluorophores were excited with a 647 nm laser; the laser power was controlled with an AOTF. A 405 nm laser was used for photoactivation. Raw images, of 40 × 40 μm, were acquired with 25 ms exposure, at 40 Hz. Each acquisition consisted of 10,000−25,000 frames.

Fluorophores were localized with Vutara software. Molecules were fitted using a measured point spread function obtained from 0.1 μm TetraSpeck Microspheres (Thermo Fisher, cat. no. T7279). The obtained molecule coordinates were exported in a .CSV file format and imported into MATLAB (MathWorks). Here, we performed drift correction in 2D and 3D using redundant cross correlation with scripts based on Wang et al.[34] Super-resolved reconstructions were rendered in 2D by plotting accumulating Gaussians with a sigma corresponding to ∼15 nm FWHM. Reconstructions were rendered with a pixel size of 20 nm for overview images;

https://doi.org/10.1021/acsomega.4c01164
ACS Omega 2024, 9, 35374−35383

zooms were rendered at a pixel size of 4 nm. 3D renders were generated by binning z-positions and plotting their positions in an image stack. The lookup table was assigned in ImageJ via temporal color coding of the hyperstacks.[35]

Data Representation and Statistical Analysis. For representative microscopy images, brightness and contrast are linearly adjusted per channel in ImageJ.[35] Statistical analysis and graphs were made using Prism (GraphPad). Final figures were composed in Affinity Designer 2 (Affinity).

■ ASSOCIATED CONTENT

Data Availability Statement

Datasets presented in the manuscript are accessible in the zenodo.org repository (DOI: 10.5281/zenodo.13171575). Extended data files are available upon request to the corresponding author(s) of the publication. We advise contacting Dr. Anne Zemella for information on in vitro synthesis and click chemistry assays and Dr. Bas van Bommel for information on microscopy experiments.

Supporting Information

The Supporting Information is available free of charge at https://pubs.acs.org/doi/10.1021/acsomega.4c01164.

Confocal and dSTORM images of NRK52E-EGFP-Septin 2 cells stained with unreacted AF647 DIBO and AF647 DIBO preincubated with AzF (PDF)

■ AUTHOR INFORMATION

Corresponding Authors

Bas van Bommel − *Institut für Chemie und Biochemie, Freie Universität Berlin, 14195 Berlin, Germany*; Email: bas.van.bommel@fu-berlin.de

Anne Zemella − *Branch Bioanalytics and Bioprocesses, Fraunhofer Institute for Cell Therapy and Immunology, 14476 Potsdam, Germany*; orcid.org/0000-0003-4895-5423; Email: Anne.Zemella@izi-bb.fraunhofer.de

Authors

Lukas Behrens − *Institut für Chemie und Biochemie, Freie Universität Berlin, 14195 Berlin, Germany; Branch Bioanalytics and Bioprocesses, Fraunhofer Institute for Cell Therapy and Immunology, 14476 Potsdam, Germany*; orcid.org/0009-0008-6967-8123

Ruben Magnus Walter − *Branch Bioanalytics and Bioprocesses, Fraunhofer Institute for Cell Therapy and Immunology, 14476 Potsdam, Germany; Institute of Biotechnology, Technische Universität Berlin, 10623 Berlin, Germany*

Weining Cai − *Institut für Chemie und Biochemie, Freie Universität Berlin, 14195 Berlin, Germany*; orcid.org/0009-0006-8664-8538

Helge Ewers − *Institut für Chemie und Biochemie, Freie Universität Berlin, 14195 Berlin, Germany*

Complete contact information is available at: https://pubs.acs.org/10.1021/acsomega.4c01164

Author Contributions

L.B., R.M.W., and B.v.B. performed the experiments. L.B., B.v.B., and W.C. made the illustrations and figures. L.B., B.v.B., H.E., and A.Z. wrote the manuscript. All authors commented on and revised the manuscript.

Funding

This work was supported by the Freie Universität Berlin and funded by the Deutsche Forschungsgemeinschaft (DFG, German Research Foundation) as part of TRR 186 (project number 278001972) to H.E. and the Ministry of Science, Research and Culture (MWFK, Brandenburg, Germany), project PZ-Syn (project number F241-03-FhG/005/001) and Fraunhofer Internal Programs under Grant No. SME 40-06962 to R.M.W. and A.Z.

Notes

The authors declare no competing financial interest.

■ ACKNOWLEDGMENTS

The authors like to thank Dr. Marina Mikhaylova for sharing the COS7 cell line and the initial DNA sequence encoding for α-tubulin and TOM20. The Lag16 anti-GFP nanobody was a kind gift of Dr. Michael P. Rout. Additionally, the authors like to thank Jeffrey Schloßhauer for providing engineered CHO-lysates for the in vitro protein synthesis. The authors would like to further express their gratitude toward the members of the institute for biochemistry and Fraunhofer IZI-BB working group "Cell-free Protein Synthesis" for their help and useful comments during group meetings.

■ REFERENCES

(1) Ackaert, C.; Smiejkowska, N.; Xavier, C.; Sterckx, Y. G. J.; Denies, S.; Stijlemans, B.; Elkrim, Y.; Devoogdt, N.; Caveliers, V.; Lahoutte, T.; Muyldermans, S.; Breckpot, K.; Keyaerts, M. Immunogenicity Risk Profile of Nanobodies. *Front. Immunol.* **2021**, *12* (March), 632687.

(2) Fridy, P. C.; Li, Y.; Keegan, S.; Thompson, M. K.; Nudelman, I.; Scheid, J. F.; Oeffinger, M.; Nussenzweig, M. C.; Fenyö, D.; Chait, B. T.; Rout, M. P. A Robust Pipeline for Rapid Production of Versatile Nanobody Repertoires. *Nat. Methods* **2014**, *11* (12), 1253−1260.

(3) Mikhaylova, M.; Cloin, B. M. C.; Finan, K.; Van Den Berg, R.; Teeuw, J.; Kijanka, M. M.; Sokolowski, M.; Katrukha, E. A.; Maidorn, M.; Opazo, F.; Moutel, S.; Vantard, M.; Perez, F.; Van Bergen En Henegouwen, P. M. P.; Hoogenraad, C. C.; Ewers, H.; Kapitein, L. C. Resolving Bundled Microtubules Using Anti-Tubulin Nanobodies. *Nat. Commun.* **2015**, *6* (1), 7933.

(4) Pronk, S. D.; Schooten, E.; Heinen, J.; Helfrich, E.; Oliveira, S.; van Bergen en Henegouwen, P. M. P. Single Domain Antibodies as Carriers for Intracellular Drug Delivery: A Proof of Principle Study. *Biomolecules* **2021**, *11* (7), 927.

(5) Moutel, S.; Bery, N.; Bernard, V.; Keller, L.; Lemesre, E.; De Marco, A.; Ligat, L.; Rain, J. C.; Favre, G.; Olichon, A.; Perez, F. NaLi-H1: A Universal Synthetic Library of Humanized Nanobodies Providing Highly Functional Antibodies and Intrabodies. *Elife* **2016**, *5* (JULY), 1−31.

(6) Markham, A. Envafolimab: First Approval. *Drugs* **2022**, *82* (2), 235−240.

(7) Morrison, C. Nanobody Approval Gives Domain Antibodies a Boost. *Nat. Rev. Drug Discovery* **2019**, *18* (7), 485−487.

(8) Keam, S. J. Ozoralizumab: First Approval. *Drugs* **2023**, *83* (1), 87−92.

(9) Chekol Abebe, E.; Yibeltal Shiferaw, M.; Tadele Admasu, F.; Asmamaw Dejenie, T. Ciltacabtagene Autoleucel: The Second Anti-BCMA CAR T-Cell Therapeutic Armamentarium of Relapsed or Refractory Multiple Myeloma. *Front. Immunol.* **2022**, *13* (September), 1−15.

(10) Ries, J.; Kaplan, C.; Platonova, E.; Eghlidi, H.; Ewers, H. A. A simple, versatile method for GFP-based super-resolution microscopy via nanobodies. *Nat. Methods* **2012**, *9* (6), 582−584.

(11) Bommel, B. v.; Konietzny, A.; Kobler, O.; Bär, J.; Mikhaylova, M. F-actin Patches Associated with Glutamatergic Synapses Control

Positioning of Dendritic Lysosomes. *EMBO J.* **2019**, *38* (15), No. e101183.
(12) Götzke, H.; Kilisch, M.; Martínez-Carranza, M.; Sograte-Idrissi, S.; Rajavel, A.; Schlichthaerle, T.; Engels, N.; Jungmann, R.; Stenmark, P.; Opazo, F.; Frey, S. The ALFA-Tag Is a Highly Versatile Tool for Nanobody-Based Bioscience Applications. *Nat. Commun.* **2019**, *10* (1), 4403.
(13) Gross, G. G.; Junge, J. A.; Mora, R. J.; Kwon, H. B.; Olson, C. A.; Takahashi, T. T.; Liman, E. R.; Ellis-Davies, G. C. R.; McGee, A. W.; Sabatini, B. L.; Roberts, R. W.; Arnold, D. B. Recombinant Probes for Visualizing Endogenous Synaptic Proteins in Living Neurons. *Neuron* **2013**, *78* (6), 971−985.
(14) Fabricius, V.; Lefèbre, J.; Geertsema, H.; Marino, S. F.; Ewers, H. Rapid and Efficient C-Terminal Labeling of Nanobodies for DNA-PAINT. *J. Phys. D Appl. Phys.* **2018**, *51* (47), 474005.
(15) Hebbrecht, T.; Liu, J.; Zwaenepoel, O.; Boddin, G.; Van Leene, C.; Decoene, K.; Madder, A.; Braeckmans, K.; Gettemans, J. Nanobody Click Chemistry for Convenient Site-Specific Fluorescent Labelling, Single Step Immunocytochemistry and Delivery into Living Cells by Photoporation and Live Cell Imaging. *N. Biotechnol.* **2020**, *59* (May), 33−43.
(16) Schloßhauer, J. L.; Cavak, N.; Zemella, A.; Thoring, L.; Kubick, S. Cell Engineering and Cultivation of Chinese Hamster Ovary Cells for the Development of Orthogonal Eukaryotic Cell-Free Translation Systems. *Front. Mol. Biosci.* **2022**, *9* (April), 832379.
(17) Mihaila, T. S.; Bäte, C.; Ostersehlt, L. M.; Pape, J. K.; Keller-Findeisen, J.; Sahl, S. J.; Hell, S. W. Enhanced Incorporation of Subnanometer Tags into Cellular Proteins for Fluorescence Nanoscopy via Optimized Genetic Code Expansion. *Proc. Natl. Acad. Sci. U.S.A.* **2022**, *119* (29), No. e2201861119.
(18) Banko, M.; Mucha-Kruczynska, I.; Weise, C.; Heyd, F.; Ewers, H. A Homozygous Genome-Edited Sept2-EGFP Fibroblast Cell Line. *Cytoskeleton* **2019**, *76* (1), 73−82.
(19) Zehtabian, A.; Müller, P. M.; Goisser, M.; Obendorf, L.; Jänisch, L.; Hümpfer, N.; Rentsch, J.; Ewers, H. Precise Measurement of Nanoscopic Septin Ring Structures with Deep Learning-Assisted Quantitative Superresolution Microscopy. *Mol. Biol. Cell* **2022**, *33* (8), ar76.
(20) Haueis, L.; Stech, M.; Kubick, S. A Cell-Free Expression Pipeline for the Generation and Functional Characterization of Nanobodies. *Front. Bioeng. Biotechnol.* **2022**, *10* (April), 1−11.
(21) Lelek, M.; Gyparaki, M. T.; Beliu, G.; Schueder, F.; Griffié, J.; Manley, S.; Jungmann, R.; Sauer, M.; Lakadamyali, M.; Zimmer, C. Single-Molecule Localization Microscopy. *Nat. Rev. Methods Primers* **2021**, *1* (1), 39.
(22) Sograte-Idrissi, S.; Schlichthaerle, T.; Duque-Afonso, C. J.; Alevra, M.; Strauss, S.; Moser, T.; Jungmann, R.; Rizzoli, S. O.; Opazo, F. Circumvention of Common Labelling Artefacts Using Secondary Nanobodies. *Nanoscale* **2020**, *12* (18), 10226−10239.
(23) Shaib, A. H.; Chouaib, A. A.; Chowdhury, R.; Mihaylov, D.; Imani, V.; Georgiev, S. V.; Mougios, N.; Reshetniak, S.; Mimoso, T.; Chen, H.; Fatehbasharzad, P.; Crzan, D.; Saal, K.; Alawar, N.; Eilts, J.; Kang, J.; Trenkwalder, C.; Mollenhauer, B.; Outeiro, T. F.; Preobraschenski, J.; Becherer, U.; Moser, T.; Edward, S.; Aricescu, A. R.; Sauer, M.; Opazo, F.; Rizzoli, S. O. Visualizing Proteins by Expansion Microscopy Abstract Fluorescence Imaging Is One of the Most Versatile and Widely-Used Tools in Biology 1. **2023**, bioRxiv:2022.08.03.502284. bioRxiv. .
(24) Wolff, J. O.; Scheiderer, L.; Engelhardt, T.; Engelhardt, J.; Matthias, J.; Hell, S. W. MINFLUX Dissects the Unimpeded Walking of Kinesin-1. *Science* **2023**, *379* (6636), 1004−1010.
(25) Kosuri, P.; Altheimer, B. D.; Dai, M.; Yin, P.; Zhuang, X. Rotation Tracking of Genome-Processing Enzymes Using DNA Origami Rotors. *Nature* **2019**, *572* (7767), 136−140.
(26) Helmerich, D. A.; Beliu, G.; Taban, D.; Meub, M.; Streit, M.; Kuhlemann, A.; Doose, S.; Sauer, M. Photoswitching Fingerprint Analysis Bypasses the 10-Nm Resolution Barrier. *Nat. Methods* **2022**, *19* (8), 986−994.
(27) Wang, R. Y. R.; Kudryashev, M.; Li, X.; Egelman, E. H.; Basler, M.; Cheng, Y.; Baker, D.; Dimaio, F. De Novo Protein Structure Determination from Near-Atomic-Resolution Cryo-EM Maps. *Nat. Methods* **2015**, *12* (4), 335−338.
(28) Boersma, Y. L.; Plückthun, A. DARPins and Other Repeat Protein Scaffolds: Advances in Engineering and Applications. *Curr. Opin. Biotechnol.* **2011**, *22* (6), 849−857.
(29) Schlichthaerle, T.; Eklund, A. S.; Schueder, F.; Strauss, M. T.; Tiede, C.; Curd, A.; Ries, J.; Peckham, M.; Tomlinson, D. C.; Jungmann, R. Ortsspezifische Funktionalisierung von Affimeren Für Die DNA-PAINT-Mikroskopie. *Angew. Chem.* **2018**, *130* (34), 11226−11230.
(30) Tiede, C.; Bedford, R.; Heseltine, S. J.; Smith, G.; Wijetunga, I.; Ross, R.; Alqallaf, D.; Roberts, A. P. E.; Balls, A.; Curd, A.; Hughes, R. E.; Martin, H.; Needham, S. R.; Zanetti-Domingues, L. C.; Sadigh, Y.; Peacock, T. P.; Tang, A. A.; Gibson, N.; Kyle, H.; Platt, G. W.; Ingram, N.; Taylor, T.; Coletta, L. P.; Manfield, I.; Knowles, M.; Bell, S.; Esteves, F.; Maqbool, A.; Prasad, R. K.; Drinkhill, M.; Bon, R. S.; Patel, V.; Goodchild, S. A.; Martin-Fernandez, M.; Owens, R. J.; Nettleship, J. E.; Webb, M. E.; Harrison, M.; Lippiat, J. D.; Ponnambalam, S.; Peckham, M.; Smith, A.; Ferrigno, P. K.; Johnson, M.; McPherson, M. J.; Tomlinson, D. C. Affimer Proteins Are Versatile and Renewable Affinity Reagents. *Elife* **2017**, *6* (c), 1−35.
(31) Hughes, L. D.; Rawle, R. J.; Boxer, S. G. Choose Your Label Wisely: Water-Soluble Fluorophores Often Interact with Lipid Bilayers. *PLoS One* **2014**, *9* (2), No. e87649.
(32) Fieller, E. C. The Biological Standardization of Insulin. *J. R. Stat. Soc.* **1940**, *7* (1), 1−64.
(33) Chin, J. W.; Martin, A. B.; King, D. S.; Wang, L.; Schultz, P. G. Addition of a Photocrosslinking Amino Acid to the Genetic Code of Escherichia Coli. *Proc. Natl. Acad. Sci. U.S.A.* **2002**, *99* (17), 11020−11024.
(34) Wang, Y.; Schnitzbauer, J.; Hu, Z.; Li, X.; Cheng, Y.; Huang, Z.-L.; Huang, B. Localization Events-Based Sample Drift Correction for Localization Microscopy with Redundant Cross-Correlation Algorithm. *Opt. Express* **2014**, *22* (13), 15982.
(35) Schneider, C. A.; Rasband, W. S.; Eliceiri, K. W. NIH Image to ImageJ: 25 Years of Image Analysis. *Nat. Methods* **2012**, *9* (7), 671−675.

https://doi.org/10.1021/acsomega.4c01164
ACS Omega 2024, 9, 35374−35383